Misfolding Pathways of the Prion Protein Probed by Molecular Dynamics Simulations

Alessandro Barducci,*† Riccardo Chelli,*† Piero Procacci,*† and Vincenzo Schettino*†
*Dipartimento di Chimica, University of Florence, Sesto Fiorentino, Italy; and †European Laboratory for Non-linear Spectroscopy, Sesto Fiorentino, Italy

ABSTRACT Although the cellular monomeric form of the benign prion protein is now well characterized, a model for the monomer of the misfolded conformation (PrP^{Sc}) remains elusive. PrP^{Sc} quickly aggregates into highly insoluble fibrils making experimental structural characterization very difficult. The tendency to aggregation of PrP^{Sc} in aqueous solution implies that the monomer fold must be hydrophobic. Here, by using molecular dynamics simulations, we have studied the cellular mouse prion protein and its D178N pathogenic mutant immersed in a hydrophobic environment (solution of CCl_4), to reveal conformational changes and/or local structural weaknesses of the prion protein fold in unfavorable structural and thermodynamic conditions. Simulations in water have been also performed. Although observing in general a rather limited conformation activity in the nanosecond timescale, we have detected a significant weakening of the antiparallel β-sheet of the D178N mutant in CCl_4 and to a less extent in water. No weakening is observed for the native prion protein. The increase of β-structure in the monomer, recently claimed as evidence for misfolding to PrP^{Sc}, has been also observed in this study irrespective of the thermodynamic or structural conditions, showing that this behavior is very likely an intrinsic characteristic of the prion protein fold.

INTRODUCTION

Prions are proteinaceous infectious particles that are probably the primary pathogens of a class of diseases known as transmissible spongiform encephalopathies (TSE) (Prusiner, 1982, 1998). These disorders are caused by the conversion of a cellular protein (PrP^{C}) into a misfolded, oligomeric isoform (PrP^{Sc}) that accumulates in plaques in the brain. The two isoforms are identical in the primary structure but differ radically in the secondary, tertiary, and quaternary structure. PrP^{C} is a GPI-anchored surface protein with an intramolecular disulfide bridge and two glycosylation sites (Prusiner, 1998; Stahl and Prusiner, 1991). The available NMR structures of PrP^{C}, mouse (Riek et al., 1996), Syrian hamster (James et al., 1997; Liu et al., 1999), human (Zahn et al., 2000), and bovine (Lopez Garcia et al., 2000), are very similar. They consist of a flexible N-terminal region and a globular domain in the C-terminal region made up of three α-helices and a short two-stranded antiparallel β-sheet (Riek et al., 1996). The PrP^{Sc} tendency to aggregate in insoluble, amorphous particles (Prusiner et al., 1983; Pan et al., 1993; Nguyen et al., 1995) has prevented the use of x-ray crystallography or NMR spectroscopy for its structure determination. The available structural data on PrP^{Sc} monomer can be summarized as follows: i), Fourier transform infrared and circular dichroism (Caughey et al., 1991; Pan et al., 1993) spectroscopies indicate that during the conversion there is a major shift in secondary structure with a relevant increase of β-structure; and ii), helices 2 and 3, along with the connecting disulfide bridge, are probably unaffected in the misfolding process (Pan et al., 1993; Prusiner, 1998). Based on these experimental evidences, two model structures for the PrP^{Sc} monomer have been proposed. In the first and older model (Huang et al., 1996), PrP^{Sc} is made up of two α-helices and a large, multi-stranded antiparallel β-sheet. A second and alternative model has been proposed by Wille et al. (2002) on the basis of a fit of trial PrP^{Sc} monomer models in 7 Å resolution two-dimensional PrP^{Sc} crystals projection maps obtained by negative stain electron microscopy. This latter model features instead a parallel β-helix and clearly implies the disintegration of the antiparallel β-sheet at some stage of the $PrP^{C} \rightarrow PrP^{Sc}$ conversion. The stability of the β-sheet in PrP^{C} (that is characterized by high dynamical plasticity even at physiological conditions; Riek et al., 1998) may therefore represent a key element for a deeper understanding of the PrP^{Sc} monomer structure.

In this work, molecular dynamics (MD) simulations have been used to reveal conformational changes and/or weaknesses of the prion protein (PrP) fold in structural and thermodynamic conditions that are experimentally known to favor PrP misfolding and aggregation. With this respect, the behavior of the β-sheet motif in pathogenic condition has been recently claimed in an MD study (Alonso et al., 2001; DeMarco and Daggett, 2004) as evidence of the presence of antiparallel β-sheet in PrP^{Sc}. This view, although being consistent with the earlier PrP^{Sc} model structure by Huang et al. (1996), does not agree with the recent parallel β-helix model proposed by Wille et al. (2002). Here we plan to shed some further light in the stability of the β-sheet of the PrP fold, hopefully providing a key of interpretation for clarifying and rationalizing the contradictory theoretical and experimental results on the structure of the misfolded PrP.

Submitted July 19, 2004, and accepted for publication November 10, 2004.

Address reprint requests to Riccardo Chelli, Tel.: 39-055-457-3082; Fax: 39-055-457-3077; E-mail: chelli@chim.unifi.it.

0006-3495/05/02/1334/10 $2.00

doi: 10.1529/biophysj.104.049882

MD simulations have become a useful and common tool for studying structural and dynamical properties of peptides and proteins. We must stress here that, even if the folding pathways of oligopeptides or small proteins have been determined in some cases by canonical MD simulations (see e.g., Duan and Kollman, 1998), the conversion between the two prion isoforms, involving a major rearrangement of the tertiary and secondary structure, is a far too slow process to be observed in conventional MD simulations. However, as done recently by other authors (Alonso et al., 2001; El Bastawissy et al., 2001; Gsponer et al., 2001; Gu et al., 2003; Sekijima et al., 2003; DeMarco and Daggett, 2004), we can gain valuable information by performing simulations of PrP^{C} using thermodynamic or structural conditions that are experimentally known to favor the misfolded isoform and by identifying structural readjustments and/or local weaknesses induced in the native fold. In particular, in two recent studies on the Syrian hamster PrP at low pH (Alonso et al., 2001; DeMarco and Daggett, 2004) a major conversion involving the build up of antiparallel β-sheet was observed, pointing to the antiparallel β-strand addition near helix 1 as the preferential pathway for the conformational conversion to PrP^{Sc}. This result, however, is at variance with the data obtained from a previous MD simulation (Sekijima et al., 2003) done on the same system and in the same thermodynamic conditions, where only a very limited tendency to β-strand elongation and/or addition was observed. Possibly the results of Alonso et al. (2001) and those of DeMarco and Daggett (2004) may be partly flawed due to artifacts induced by their treatment of electrostatics based on the simple and substandard protocol of spherical truncation (Saito, 1994; Cheatham et al., 1995; Wolf et al., 1999; Patra et al., 2003), and/or by the neutralization scheme (Monticelli and Colombo, 2004) of the highly charged PrP at low pH.

In this article, we have performed MD simulations of the mouse PrP ($mPrP^{C}$) adopting the following ''perturbing conditions'': i), from the thermodynamic standpoint, we choose an apolar environment (solution of CCl_4) as PrP^{Sc} (and hence PrP^{Sc} monomer) is known to be extremely hydrophobic (Prusiner et al., 1981; Pan et al., 1993), and ii), from the structural point of view, we choose to introduce the D178N point mutation that is known to be associated with two different strains of inherited TSE (Prusiner, 1996) and to drastically lessen the thermodynamic stability of PrP^{C} fold (Liemann and Glockshuber, 1999).

It is generally assumed (Fraunfelder et al., 1988) that the free energy surface of solvated proteins has many local free energy minima that are often separated by large barriers. In such circumstances, the sampling power of the phase space by a single conventional MD trajectory is very limited. As a consequence, two simulations of a system in the same thermodynamic conditions that start from the same nonequilibrium state and that differ only in, e.g., the thermalization scheme, may yield different results and hence lead to contradictory conclusions. With this respect, the nonergodic behavior of $mPrP^{C}$ and its D178N mutant in standard conditions has been recently pointed out (Gsponer et al., 2001). In this study, to lessen the impact of the inherent nonergodicity of solvated proteins, we generate a ''swarm'' of independent and few ns long trajectories for each given protein-solvent system. In fact, the MD approach proposed here is aimed at studying the stability of the structural motifs of the $mPrP^{C}$ in conditions that favor conversion to PrP^{Sc} and under the assumption that solvent induced or local structure driven transitions between minima are fast processes, but rare events (Duan and Kollman, 1998). Under these assumptions and in this nonequilibrium framework, the proposed simulation protocol should allow in principle and in practice (Gsponer et al., 2001) a better sampling of the phase space with respect to the single long trajectory approach, as the productive part of a single and longer trajectory would probably stay trapped in the same minimum.

The outline of the article is the following: in ''Methods'', we report the computational details common to all MD simulations (the details about the different thermalization procedures we used are described in ''Results''). The analysis of the MD trajectories is reported in ''Results''. A deep discussion of the results is given in ''Discussion''. To further support our results, structural analysis of NMR conformers of the human PrP at pH 4.5 and 7.0 is reported and discussed in ''Discussion''. Conclusions and perspectives are given in ''Conclusions''.

METHODS

All the simulations presented in this article began with the $mPrP^{C}$ NMR structure from the Brookhaven Protein Data Bank (PDB) (Bernstein et al., 1977) that contains the coordinates of the residues 124–226 (PDB code: 1AG2). The simulations were done using the ORAC program (Procacci et al., 1997) and were carried out in the isothermal-isobaric ensemble ($P = 0.1$ MPa, $T = 293$ K) using a cubic box with standard periodic boundary conditions. Temperature control is achieved using a Nosé thermostat (Nosé, 1984), whereas constant pressure is imposed using a modification of the Parrinello-Rahman Lagrangian (Marchi and Procacci, 1998). The solvent is made up of 1176 CCl_4 molecules or 5226 water molecules. The protein was modeled using the AMBER force field (Cornell et al., 1995). The disulfide bridge was described by a covalent bond. Experimental evidences (Turk et al., 1988) show in fact that the disulfide bridge remains oxidized in PrP^{Sc}. The potential parameters for CCl_4 molecules were those proposed by Fox and Kollman (1998), whereas TIP3P model (Jorgensen et al., 1983) was used for water. The Ewald method with the smooth particle mesh algorithm (Essmann et al., 1995) was used to compute electrostatic interactions. The grid spacing in each dimension of the direct lattice was $\sim$0.9 Å, whereas the Ewald convergence parameter was set to 0.43 $Å^{-1}$. The electroneutrality of the simulation box was achieved by adding a countercharge (2 e for the wild-type PrP and 1 e for the D178N mutant) that was smeared onto all the protein atoms. An r-RESPA multi-step algorithm (Tuckerman et al., 1992) with a potential subdivision specifically tuned for proteins (Procacci et al., 1996) was used for integrating the equations of motion. The thermalization procedure is in general made up of two phases: in the first one only the solvent is relaxed, whereas the protein atoms are kept fixed to their experimental coordinates. In the second phase also the protein atoms are gradually relaxed. More details about the thermalization procedure for the various classes of simulations, *l*, *a*, and *m* are given in the next section.

RESULTS

A summary of the salient data of the simulations is reported in Table 1. The *l*-class simulations (*l*-WT-CCl_4 and *l*-D178N-CCl_4) are two runs of the wild-type (WT) $mPrP^C$ and of its D178N mutant in CCl_4 with a thermalization phase of 2.7 ns and a production run of 5.4 ns. The *a*-class simulations (*a*-WT-CCl_4 and *a*-D178N-CCl_4) are four independent runs of WT $mPrP^C$ and of its D178N mutant performed in CCl_4, each with a 2.5-ns thermalization phase and a production run of 2.4 ns. In the *a*-class simulations, the system was prepared as follows: after thermalization of the solvent and of the side chains, the system was completely relaxed, suddenly heated up to 368 K and then gradually cooled down to 293 K at a rate of 0.047 K ps^{-1}. This thermalization protocol was used for increasing the possibility of escaping local free energy minima thus improving the sampling power of the simulations. The starting configurations for the mutant in the *l*- and *a*-class simulations are generated by replacing randomly one of the carboxylic oxygen atoms of Asp-178 with an NH_2 group. The *m*-class simulations, *m*-WT-CCl_4 (WT PrP in CCl_4), *m*-D178N-CCl_4 (D178N mutant in CCl_4), *m*-WT-H_2O (WT PrP in water), and *m*-D178N-H_2O (D178N mutant in water), refer each to a swarm of eight independent runs. Each run is 3 ns long (1.2 ns being used for thermalization) for a total length of 24 ns per swarm of simulations. In the *m*-D178N-H_2O and *m*-D178N-CCl_4 runs, the point mutation D178N was introduced during the thermalization phase by linearly varying in $\sim$100 ps the potential parameters (Lennard-Jones parameters and atomic charges) from the values associated with an aspartic acid to those associated with an asparagine.

Root mean-square displacements (RMSDs) of α-carbons from the experimental PrP structure are also reported in Table 1. In all the simulations, the RMSDs, after an increase in few hundreds femtoseconds during the thermalization phase, reach a stable plateau. This behavior is similar to that observed in other MD studies on PrP (Gsponer et al., 2001) and is typical of equilibrium or quasi-equilibrium systems. In denaturing conditions (CCl_4), quasi-equilibrium states probed by converged RMSDs correspond to local free energy minima that cannot be easily escaped in the simulation timescale. In Table 1, we collect some cumulative data concerning the average RMSDs, along with corresponding standard deviations obtained for the simulations listed in the table. The RMSDs for WT PrP in water solution (*m*-WT-H_2O in Table 1) are comparable to those reported in other MD studies of mPrP (Guilbert et al., 2000; El Bastawissy et al., 2001; Gsponer et al., 2001). For simulations performed in CCl_4 (entries *l*-WT-CCl_4, *l*-D178N-CCl_4, *a*-WT-CCl_4, *a*-D178N-CCl_4, *m*-WT-CCl_4, *m*-D178N-CCl_4 in Table 1), given the destabilizing effect of the hydrophobic environment, the mean RMSDs are found to be larger. In fact, runs of mPrP in CCl_4 are technically off-equilibrium simulations as they refer to an equilibrium solute structure fit for water immersed in apolar solvent. Despite the enhanced protein mobility in CCl_4 with respect to water, the presence of the plateau in the RMSD time record shows that cellular $mPrP^C$ does not undergo appreciable unfolding in a nanosecond timescale even when abruptly immersed in apolar environment unfit for its fold. The mean RMSD values of the *l*-WT-CCl_4 and *l*-D178N-CCl_4 runs are comparable to those of the *m*-WT-CCl_4 and *m*-D178N-CCl_4 simulations, showing that an increase in the simulation length in a nanosecond timescale may not result in an appreciable improvement of the configuration space sampling. This conclusion is confirmed by the small RMSD fluctuations observed in each independent simulation, irrespective of the simulation class *a*, *l*, *m* ($\overline{\sigma_t}$ in Table 1), clearly indicating that a single trajectory in a nanosecond timescale can explore only a limited region of the phase space around a local free energy minimum. On the contrary, the RMSD standard deviations, computed by averaging over the entire simulation time of the swarm (σ_T in Table 1), are sensibly larger for *a*-class and *m*-class simulations. This result indicates that running independent set of simulations effectively enhances the sampling capability of conformational space in PrP, as largely expected and as recently reported by other authors

TABLE 1 C_α root mean-square deviations of PrP for various classes of simulations (see Results for details)

Simulation class	*n*	*t*	*T*	RMSD	$\overline{\sigma_t}$	σ_T
l-WT-CCl_4	1	8.1 (2.7)	8.1	2.6	0.06	0.06
l-D178N-CCl_4	1	8.1 (2.7)	8.1	2.7	0.15	0.15
a-WT-CCl_4	4	4.9 (2.5)	19.6	3.3	0.09	0.36
a-D178N-CCl_4	4	4.9 (2.5)	19.6	3.7	0.10	0.28
m-WT-CCl_4	8	3.0 (1.2)	24.0	2.8	0.14	0.43
m-D178N-CCl_4	8	3.0 (1.2)	24.0	2.4	0.13	0.28
m-WT-H_2O	8	3.0 (1.2)	24.0	2.4	0.18	0.31
m-D178N-H_2O	8	3.0 (1.2)	24.0	2.5	0.17	0.28

n, number of independent runs.
t, simulation time (ns) for each independent run (thermalization length in parenthesis).
T, total simulation time (ns).
RMSD, root mean-square deviation (Å) averaged over the independent runs.
$\overline{\sigma_t}$, standard deviation (Å) of the RMSD averaged over the independent runs.
σ_T, standard deviation (Å) of the RMSD computed over the total simulation time *T*.

(Gsponer et al., 2001). The largest RMSDs are observed in the *a*-class runs and are likely caused by the high temperature experienced by the system during the thermalization phase. In fact, the transient high temperature regime and the subsequent annealing to normal conditions provide the necessary activation energy to overcome the barriers between proximal local free energy minima.

The importance of the secondary structure stability for identifying local weaknesses and/or early stages for conversion pathways to PrP^{Sc} has already been stressed in the introduction. The secondary structure was analyzed by using the DSSP program (Kabsch and Sander, 1983). Fig. 1 shows the protein secondary structure averaged over all the *m*-class simulations for each protein-solvent system. In the simulations performed in water, the three α-helices (Fig. 1 *a*) are preserved and close to the experimental pattern for both WT PrP and D178N mutant. The isosteric replacement of the residue 178 in water is apparently unable to affect the α-helices stability. In fact, the differences between the WT PrP and the D178N mutant behavior are generally within the statistical error. The partial instability of the helical regions 170–175 and 218–223 and the elongation of the helix 2 on its C-terminal side are features that have been observed also in other MD studies of $mPrP^{C}$ (Guilbert et al., 2000; Gsponer et al., 2001).

Fig. 1 shows in general that the antiparallel β-sheet, which is made up of two residues strands (129–130 and 162–163) in the NMR structure, involves systematically three residues. This feature is observed for the WT PrP and the D178N mutant in both water (Fig. 1 *b*) and CCl_4 (Fig. 1 *d*). The

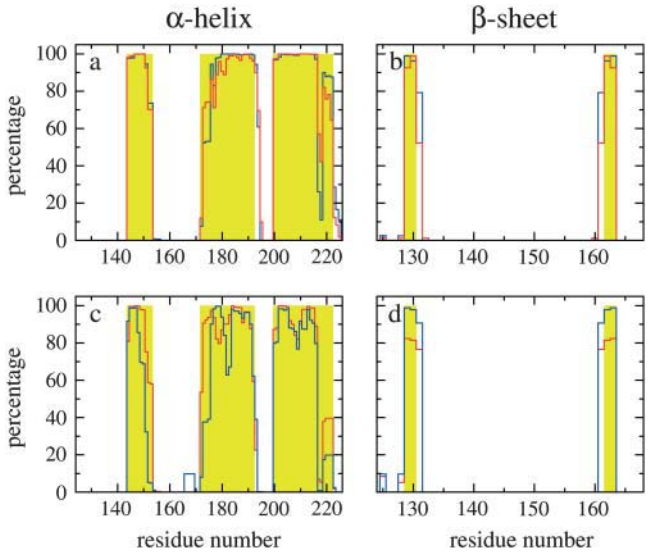

FIGURE 1 Percentage of secondary structure per residue during the productive phase of *m*-class simulations. (*Top*) Secondary structure in water ((*a*) α-helices; (*b*) β-sheets). (*Bottom*) Secondary structure in CCl_4 ((*c*) α-helices; (*d*) β-sheets). Blue and red lines indicate the wild-type PrP and its D178N mutant, respectively. The shaded yellow areas correspond to the experimental structure (Riek et al., 1996).

β-sheet elongation seems to be slightly favored in CCl_4 solution. This is to be expected considering that the CCl_4 cannot solvate effectively backbone amide and carbonyl groups and it should thus favor intrachain hydrogen bonds (H-bonds). The small bump near the N-terminal region in Fig. 1, *b* and *d*, is again a common feature for all protein systems although more evident in CCl_4, and is indicative of episodic formation of an additional third β-strand in the N-terminal disordered region that adds up to the preexisting β-sheet. The antiparallel β-sheet elongation has been observed in many other simulation studies of PrP^{C} and/or some of its mutants in different conditions (Alonso et al., 2001; Gu et al., 2003; Sekijima et al., 2003). Recently the addition of one (or more) β-strand(s) has been reported by Guilbert et al. (2000), Alonso et al. (2001), and DeMarco and Daggett (2004). DeMarco and Daggett observed both β-strand elongation and addition during a single 20-ns simulation of Syrian hamster PrP^{C} in water at low pH. As the acidic environment seems to experimentally induce PrP^{Sc}-like structures (Swietnicki et al., 1997, 2000; Hornemann and Glockshuber, 1998; Zou and Cashman, 2002), the authors identified in the antiparallel β-structure increase the first step of the $PrP^{C} \rightarrow PrP^{Sc}$ conversion. Our data suggests that both a slight β-sheet elongation and the formation of an additional β-strand might be a common event, typical of the cellular PrP fold and essentially uncorrelated with pathogenic structural (mutation D178N) or thermodynamic (CCl_4 solution) conditions. This natural tendency of $mPrP^{C}$ structure to elongate the β-structure on the flexible and disordered side could be enhanced for other PrP^{C} fragments (Syrian hamster, human) that are characterized by longer and more flexible N-terminus (Parchment and Essex, 2000).

The α-helices were markedly less preserved during the simulations in CCl_4 (see Fig. 1 *c*). The lessened stability of these structural elements is very likely caused by the apolar environment. The CCl_4 solvent may in fact interfere with the concurrent interactions among hydrophobic side chains that stabilize the protein core in experimental $mPrP^{C}$. As previously stated, the RMSD values indicate that the change of polarity is unable to induce major conformational changes in $mPrP^{C}$. However, Fig. 1 *c*, when compared to the counterpart in water, shows clearly that, in CCl_4, statistically significant local distortions are important even in a nanosecond timescale, affecting seriously the stability of secondary structure elements of the PrP. These distortions are surprisingly more significant for the WT PrP in the helical regions, whereas the β-sheet appears to be rather stable. The situation is reversed for the mutant where the α-helical regions, especially helix 1 and helix 2, are markedly more stable than those found in the WT PrP, whereas the β-sheet, despite the occasional elongation or addition, appears appreciably weakened. This split behavior of the stability of β-structure and helix structure for the mutant and WT PrP in CCl_4 is fully confirmed by *l* (see *top panel* of Fig. 2) and *a*-class simulations (data not shown).

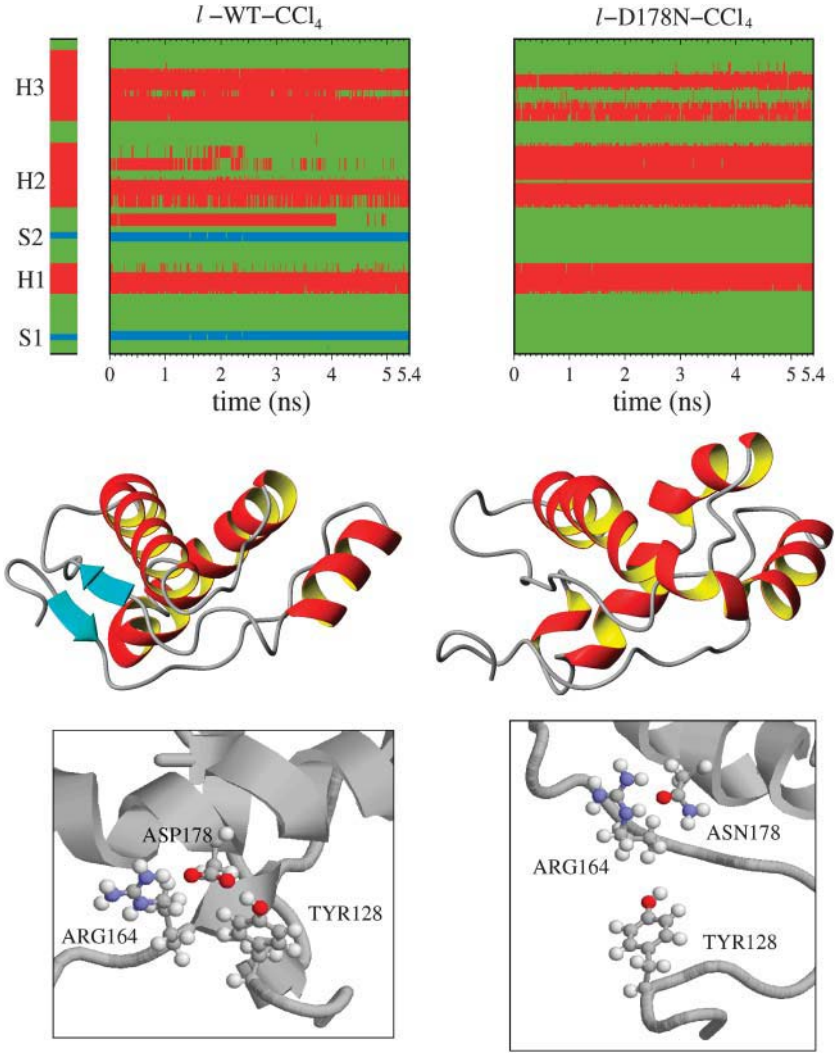

FIGURE 2 (*Top panels*) Evolution of the secondary structure during the productive phase of the *l*-WT-CCl_4 and *l*-D178N-CCl_4 simulations. The bar on the left corresponds to the experimental structure. The α-helices are shown in red; the β-sheet in blue color. (*Middle panels*) representative PrP configurations (in the secondary structure representation) taken from the *l*-WT-CCl_4 and *l*-D178N-CCl_4 simulations. (*Bottom panels*) ball-and-stick representation focused on the three residues, Arg-164, Asp-178/Asn-178, and Tyr-128, for highlighting the role played by the D178N point mutation (note that the orientation of PrP is not the same with respect to the full PrP views reported in the middle panels).

The strong weakening of the β-sheet (see Fig. 1 *d*) is observed only for the mutant in CCl_4. By inspecting the DSSP time record in each of the eight runs (data not shown), we find that this weakening occasionally corresponds to a real breakup with the two strands drifting few Å apart. This breakup is a fast event (usually occurring during thermalization or at the beginning of the productive simulation phase) but also a rare event. In fact the complete breakup of the β-sheet has been luckily observed for the *l*-D178N-CCl_4 simulation (see *top right panel* of Fig. 2), but it occurred only once in the *a*-D178N-CCl_4 runs and once in the eight *m*-D178N-CCl_4 runs.

We want to remark that the stability of the α-helices may have been possibly overestimated due to force field artifacts, both in water and in CCl_4. Indeed the force field we used (Cornell et al., 1995) has been found biased toward α-helical conformation by several authors (Garcia and Sanbonmatsu, 2002; Duan et al., 2003; Okur et al., 2003). Actually all state-of-the-art force fields are subject to such secondary structure artifacts (Mu et al., 2003; Zaman et al., 2003). Given this caveat, we have chosen the AMBER force field which is widely used and publicly available for such scrutiny. However our main findings are based on the comparison between fold behavior in different structural/thermodynamic conditions. Hence the focus is on the relative rather than absolute stability of secondary structure elements.

The stability of the β-sheet in destabilizing and pathogenic conditions, that is the central issue of this study, can be evaluated in a more accurate way by devising a structural time-dependent function that continuously varies with the extension and strength of the stack of concurring H-bonds connecting the two β-strands. To this end, we therefore define the function

$$m = -\sum_{i=1}^{N_{hb}} \cos(\theta_i)\, s(R_i), \qquad (1)$$

where the sum runs over the four ($N_{hb} = 4$) H-bonds connecting the strands 129–131 and 161–163, θ_i and R_i are the O $\cdots$ H-N angle and the O $\cdots$ H distance, respectively, of the *i*th H-bond and $s(R_i)$ is a switching function defined as follows

$$S(R) = \begin{cases} 1 & for \quad R \le 1.8 \text{ Å} \\ 1.157R^3 - 8.330R^2 + 18.742R - 12.494 & for \quad 1.8 < R \le 3.0 \text{ Å} \\ 0 & for \quad R > 3.0 \text{ Å} \end{cases}. \tag{2}$$

In Fig. 3 we report the time record of $f_\beta = m/m_{\text{exp}}$, where m_{exp} equals the function m (Eq. 1) computed using the NMR experimental structure. The function f_β is ≥ 1 when the β-sheet is stable or undergoes an elongation and/or strengthening, and is equal to zero when the two strands are completely detached. The f_β values obtained during the m-class runs are shown in Fig. 3. As far as the WT PrP is concerned, during all runs both in water (Fig. 3 *c*) and CCl_4 (Fig. 3 *a*), the f_β values are always slightly >1 showing that this structural element is stable in a nanosecond timescale in both water and apolar environment. For the case of the mutant in CCl_4 (Fig. 3 *b*), the behavior of f_β is in close agreement with the results of DSSP analysis. Fig. 3 confirms that the combined effect of the apolar environment and of the D178N mutation weakens the antiparallel β-sheet leading in some cases to its breakup. A β-sheet destabilizing effect was observed, to a smaller extent, also for the D178N mutant runs performed in water solution (Fig. 3 *d*). The f_β curves associated with the productive phases of the *a*-WT-CCl_4 and *a*-D178N-CCl_4 simulations are shown in Fig. 4. The trends are in agreement with the results obtained from the *m*-class simulations analysis, showing clearly the weakening of the β-sheet when the point mutation is introduced. Regardless of the final values, at the beginning of the productive phase all the mutant runs were characterized by a relevant destabilization of the β-sheet, even larger than that observed for the *m*-class runs. This is probably due to the fact that the heating/annealing thermalization scheme allows exploring more effectively local free energy minima for the non-equilibrium runs.

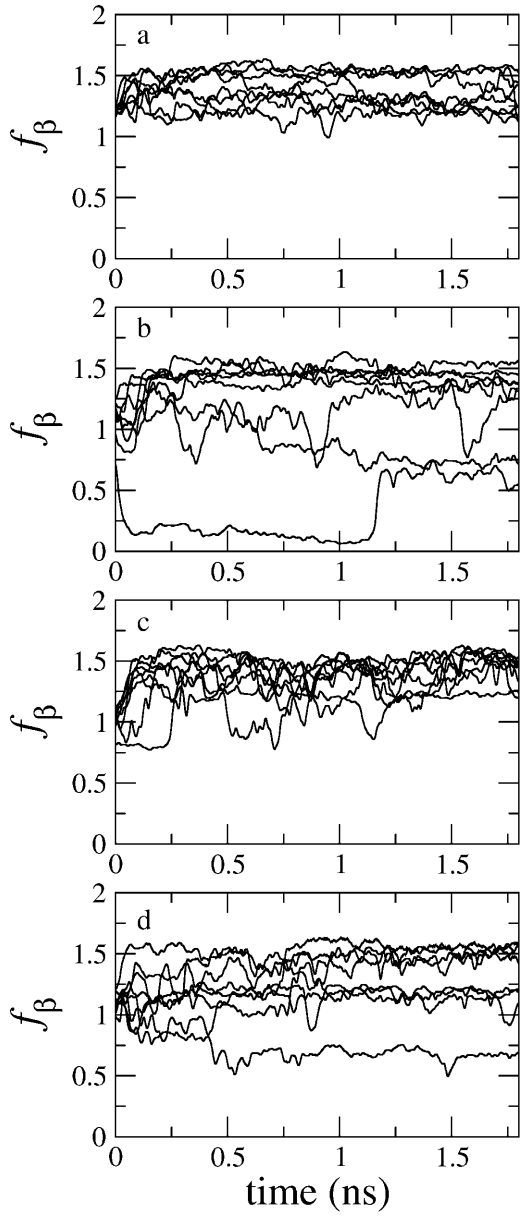

FIGURE 3 f_β values as a function of time during the productive phase of the *m*-class simulations: (*a*) *m*-WT-CCl_4, (*b*) *m*-D178N-CCl_4, (*c*) *m*-WT-H_2O, and (*d*) *m*-D178N-H_2O.

Summarizing, for the WT PrP the β-sheet is stable in both water and CCl_4, in the latter solvent involving systematically three residues per β-strand and occasionally a third β-strand on the flexible N-terminus. For D178N mutant, the β-sheet is slightly weakened in water and significantly destabilized in CCl_4 where it may occasionally break down. α-helices are in general less stable in CCl_4 with respect to water. Whereas helix 3 behaves similarly for both WT and D178N mutant, in CCl_4 helix 1 and 2 are found to be significantly more stable for the D178N mutant with respect to WT PrP. The stabilization of helices 1 and 2 of the mutant in CCl_4 implies the concurrent breakup of the β-sheet.

DISCUSSION

The basic question one could put after knowing the results of the prior section is the following: why does the D178N mutation selectively weaken the β-sheet and simultaneously reduce the solvent induced distortion in the α-helical regions? In Fig. 2 we report the secondary structure computed for the *l*-class runs (*top panels*) along with two representative PrP snapshots (*middle panels*). As shown in the bottom left panel, Asp-178 in the WT PrP lies in helix 2

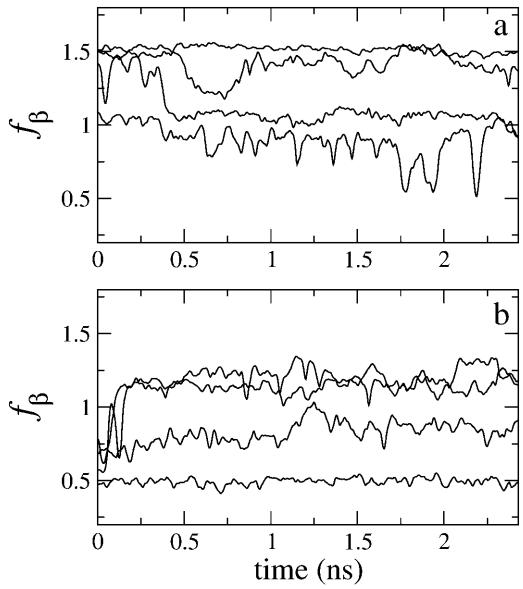

FIGURE 4 f_β values as a function of time during the productive phase of the *a*-class simulations: (*a*) *a*-WT-CCl_4 and (*b*) *a*-D178N-CCl_4.

and forms two strong electrostatic interactions, a salt bridge with the guanidino group of Arg-164 and an H-bond with the hydroxy group of Tyr-128. Tyr-128 and Arg-164 are adjacent to the β-strands S1 (129–130) and S2 (162–163), respectively. In the NMR PrP fold, Asp-178 hence holds the two β-strands close together and anchors them, along with the bracketed helix 1, to the protein core. When the mutation D178N is introduced, the negative charge on Asp-178 is lost. The mutation may hence induce the breaking of one of the two electrostatic hooks thus easing the breaking of the β-sheet (as observed in the *right top panel* of Fig. 2) with consequent destabilization of the native tertiary structure. In the mutant, the loss of the electrostatic hook that stabilizes the PrP WT fold must also help to reduce the hydrophobic structural stresses induced by the apolar solvent on the native structure. This eventually yields a decrease of mechanical constraints on helices 1 and 2 with their consequent enhanced stabilization. The complete absence of β-structure observed in the *l*-D178N-CCl_4 run (see *right top panel* of Fig. 2) can be ascribed to the loss of the interaction between Asn-178 and Tyr-128.

There might be other mechanisms for β-sheet weakening or break-up. For example, in one *a*-class simulation, the mutation-driven loss of the salt bridge between Asn-178 and Arg-164 provided an alternative route for the β-sheet loosening or breakup. Also in the *l*-D178N-CCl_4 run, as already noticed in the cumulative averages reported in Fig. 1, we can see an appreciable stabilization of helix 1 and helix 2 when the β-sheet is broken. We stress here that, irrespective of how the sample was prepared (standard thermalization, thermal annealing or morphing), the β-sheet weakening or breakup has been observed only when two combining pathogenic conditions, i.e., immersing PrP in CCl_4 and introducing the D178N point mutation, are simultaneously applied. In water the weakening of the β-sheet due to point mutation is also observed but to a less extent (see Fig. 3 *d*). A significant weakening of β-structure has been recently observed experimentally in a NMR study of human PrP at low pH (Calzolai and Zahn, 2003). In fact, like the point mutation D178N, the protonation of Asp-178 at low pH may imply the breakup of either the salt-bridge with Arg-164 or the H-bond with Tyr-128 (this issue will be addressed below in greater detail).

The β-sheet instability appears therefore to be essentially induced by the D178N point mutation, that in turn implies a weakening of the electrostatic double hook provided by the Asp-178 residue in the WT PrP (Riek et al., 1998). This mutation induced instability of the β-sheet motif may lead to its full disintegration, even in a nanosecond timescale, if the process is thermodynamically activated by abruptly immersing the mutant in an apolar environment (i.e., imposing thermodynamic conditions where the misfolded monomeric form is very likely more stable with respect to the native structure). In fact, in CCl_4, the instability of the antiparallel β-sheet motif in the mutant is enhanced and disintegration occurs with higher probability as the hydrophobic residues involved in this structural element experience solvation forces that tend to bring them on the protein surface.

In summary, the stability of the β-sheet in PrP appears to be related to the H-bond network among the side chains of the residues Tyr-128, Asp-178, and Arg-164. The introduction of the D178N point mutation, mainly since it makes the charged residue 178 electroneutral, weakens the mutual interactions among these three residues. In principle a similar effect could be also achieved lowering the solution pH. In fact, since the Asp-178 residue is exposed to the solvent, a strong acidic environment could enhance the protonation of its carboxylic group, consequently decreasing its average net charge. To get further insight for supporting our results, we have applied the f_β algorithm (see Results) to the NMR conformers of human PrP (hPrP) determined at pH 4.5 (Zahn et al., 2000) (20 conformers in the PDB; code 1QM3) and at pH 7.0 (Calzolai and Zahn, 2003) (20 conformers in the PDB; code 1HJN). In Fig. 5 *a* we report the nonnormalized *m* function (see Eq. 1) instead of the normalized f_β to allow a direct quantitative comparison of the β-sheet stability at pH 7.0 and 4.5. We clearly note that the contents in β-sheet increase with increasing pH, implying a larger stability of the β-sheet at pH 7.0. This result is consistent with the conclusions by Calzolai and Zahn (2003) obtained by evaluating the free energy of exchange of backbone amide atoms of hPrP. To get information on the hypothesized correlation between β-sheet stability and interactions among Tyr-128, Asp-178, and Arg-164, we have calculated the two atom-atom OD-OH and OD-CZ distances, where OD is the oxygen atom of the Asp-178 side chain closest to the oxygen atom (labeled OH in the PDB) of

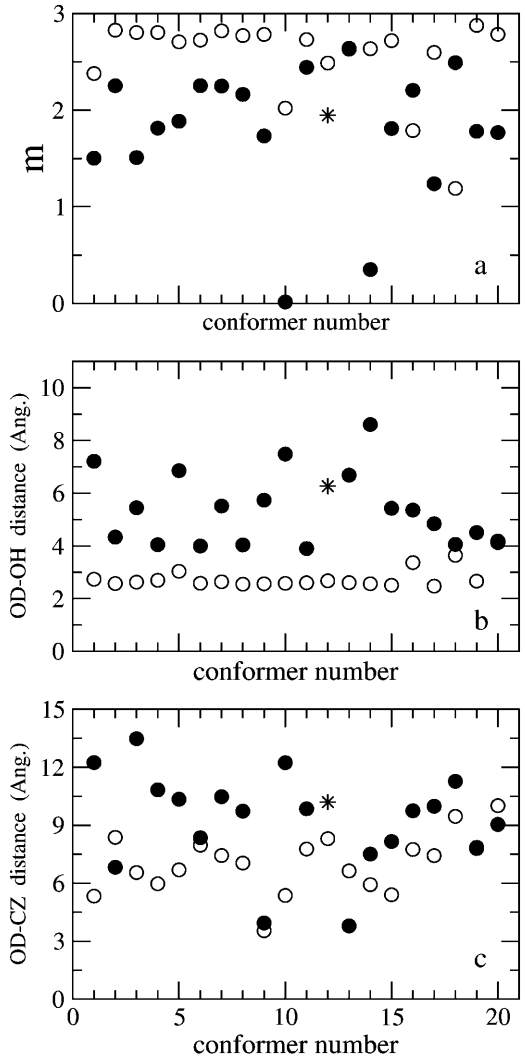

FIGURE 5 Correlation between β-sheet stability and interresidue interactions involving the Asp-178 residue in hPrP at pH 4.5 and 7.0. The data have been obtained analyzing the 20 NMR conformers reported in the PDB for each pH (PDB codes 1QM3 and 1HJN for pH 4.5 and 7.0, respectively). The conformer numbering of the PDB files has been used. Solid and open circles refer to pH 4.5 and 7.0, respectively. In the header of the PDB file, the conformer 12 at pH 4.5 is indicated as the most representative one (*asterisk* in the panels). No representative conformer has been indicated for hPrP at pH 7.0. (*a*) *m* function (see Eq. 1) showing the β-sheet stability. (*b*) OD-OH distance (see text for the label definition) showing the interaction between Asp-178 and Tyr-128 residues. (*c*) OD-CZ distance (see text for the label definition) showing the interaction between Asp-178 and Arg-164 residues.

the Tyr-128 side chain and to the carbon atom (labeled CZ in the PDB) of the Arg-164 side chain, respectively. The data are shown in Fig. 5, *b* and *c*, for all NMR conformers at both pH values. In general we can observe that for both types of interactions, Asp-178–Arg-164 (OD-CZ distance) and Asp-178–Tyr-128 (OD-OH distance), lower pH is correlated to larger interresidue distances, i.e., weaker interaction. In particular it is remarkable that the H-bond between Asp-178 and Tyr-128 is broken at low pH (see Fig. 5 *b*). The weakening of the interaction between Arg-164 and Asp-178 at low pH (see Fig. 5 *c*) is not as important as that observed for Asp-178–Tyr-128, though well evident in this case too. Although the OD-CZ distance in two conformers at pH 4.5 (conformers 9 and 13 in Fig. 5 *c*) is very short (lower than 4 Å), in the most representative conformer, indicated by the authors to be the conformer 12 (see header in the 1QM3 PDB file), such distance is predicted to be much larger, i.e., ~10.2 Å. Also the OD-OH distance (Fig. 5 *b*) in the most representative conformer at pH 4.5 is very large (~6.3 Å). No representative conformer has been indicated for the hPrP at pH 7.0 (see header in the 1HJN PDB file). These results are fully consistent with the main finding of our MD simulation study, thus offering a further experiment-based support to our results.

CONCLUSIONS

We have studied the stability of the PrP fold in various thermodynamic and structural conditions by using molecular dynamics simulations. In particular, the mouse wild-type PrP and its D178N mutant have been studied in both water and CCl_4 at room conditions. To enhance the sampling of the conformational phase space and to reduce the bias from the initial conditions, we have produced swarms of independent simulations few nanoseconds long for each protein-solvent system using different thermalization protocols. The total simulation time span for each protein-solvent system is 24 ns in water and ~52 ns in CCl_4. Results indicate that the PrP fold in the nanosecond timescale is stable and does not undergo major conformational changes, irrespective of the solvent polarity and pathogenic point mutation. We have measured the stability of secondary structure elements by means of the DSSP method and by devising an appropriate function based on geometrical considerations for measuring H-bond strength. In general the β-sheet appears to be less stable in the D178N mutant. More surprisingly, the instability of the β-sheet is enhanced in CCl_4, where intrasolute electrostatic interactions should be in principle favored with the formation of additional secondary structure. The instability of the β-sheet in the D178N mutant appears to be correlated, in CCl_4, to a corresponding stabilization of the α-helices (especially helices 1 and 2). These observations could be rationalized as follows. In the native fold, the electrostatic interactions between Arg-164, Tyr-128, and Asp-178 stabilize both the β-sheet and, partly, the PrP fold. When Asp-178 is replaced with Asn-178, helix 2 becomes less tightly bound to the antiparallel β-sheet because of the breakup either of the salt bridge Arg-164–Asp-178, or of the H-bond Tyr-128–Asp-178. The hydrophobic shock induced by the immersion in CCl_4 of the mutant of a fold fit for water and the weakening of the electrostatic hook between helix 2 and the β-strands, produces mechanical tensions leading to an effective weakening of the short antiparallel β-sheet. For some runs in CCl_4, the β-sheet breaks down easing the

tension on the PrP fold, thus allowing the stabilization of the α-helical motifs.

The correlation existing between β-sheet stability and strength of the interactions among the residues Tyr-128, Asp-178, and Arg-164 is an important issue of our study. To get further support to such observation, we have analyzed several NMR conformers of human PrP experimentally determined at pH 4.5 and 7.0. In particular we have focused on the β-sheet stability and on the strength of interaction of the residue pairs Arg-164–Asp-178 and Tyr-128–Asp-178 in terms of atom-atom distances. This analysis, seemingly uncorrelated to our specific aim, has been performed on the basis of the hypothesis that acidic environment acts similarly to the D178N point mutation. In fact, since the Asp-178 side chain is exposed to the solvent, a low pH can certainly enhance the protonated form of Asp-178. As a consequence of this increased protonation we might observe a weakening of the interaction of Asp-178 with both Arg-164 (salt bridge) and Tyr-128 (H-bond) and, at the same time, a decrease of the β-sheet stability. This is indeed what we have observed for the human PrP.

Moreover, in agreement with other MD studies, we have also observed that the small antiparallel β-sheet 129–130/162–163 may occasionally become elongated and/or undergo a β-strand addition from the flexible N-terminus. However, this phenomenon is observed in both water and CCl_4 and for both the native and the mutant PrP. Hence, our results suggest that the tendency to β-sheet elongation and/or strand addition is a typical feature of the normal monomer PrP fold in the nanosecond or submicrosecond timescale, rather than defining a possible early pathway to $PrP^{C} \rightarrow PrP^{Sc}$ conversion, as claimed elsewhere (DeMarco and Daggett, 2004).

A statistically significant weakening (and occasionally a breakup) of the antiparallel β-sheet is observed exclusively when thermodynamic and structural conditions that favor the pathogenic conversion are simultaneously applied. These observations are consistent with the following picture: at some stage during the $PrP^{C} \rightarrow PrP^{Sc}$ conversion, the antiparallel β-structure of the native fold is dissolved allowing the molecule to partially unfold; β-structure (whether parallel or antiparallel) could be then reformed in a later step. This picture and the underlying simulation data presented in this study are consistent with NMR studies on H-PrP flanking sequences encompassing helix 1 (Ziegler et al., 2003) and with the model structure for PrP^{Sc} monomer proposed recently by Wille et al. (2002), based on parallel β-helical structure extending from the N-terminus up to the second α-helix. We would further stress here that our results are not actually incompatible with antiparallel β-sheet composition of PrP^{Sc}. However they clearly suggest that, even in the case the PrP conformational transition leads to an effective formation of a multistranded antiparallel β-sheet, the unfolding mechanism should not involve the growth of the antiparallel β-sheet of PrP^{C}, as claimed in earlier MD simulation studies (Alonso et al., 2001; DeMarco and Daggett, 2004).

Although we believe that our MD approach is statistically more reliable than the standard single trajectory method, we are well aware that some kind of non-Boltzmann sampling methodology must be used to further validate our results. With this respect, we are currently applying the recently proposed history dependent metadynamic method (Laio and Parrinello, 2002) for computing the potential of mean force of β-sheet formation/disruption of WT and mutant PrP in various solvents. Results will be presented in a forthcoming article.

This work was supported by the Italian Ministero dell'Istruzione, dell'Università e della Ricerca and by the European Union (contract No. HPRI-CT-1999-00111).

REFERENCES

Alonso, D. O., S. J. DeArmond, F. E. Cohen, and V. Daggett. 2001. Mapping the early steps in the pH-induced conformational conversion of the prion protein. *Proc. Natl. Acad. Sci. USA.* 98:2985–2989.

Bernstein, F. C., T. F. Koetzle, G. J. B. Williams, E. F. Meyer, M. D. Brice, J. R. Rogers, O. Kennard, T. Shimanouchi, and M. Tasumi. 1977. The Protein Data Bank: a computer based archival file for macromolecular structures. *J. Mol. Biol.* 112:535–542.

Calzolai, L., and R. Zahn. 2003. Influence of pH on NMR structure and stability of the human prion protein globular domain. *J. Biol. Chem.* 278:35592–35596.

Caughey, B. W., A. Dong, K. S. Bhat, D. Ernst, S. F. Hayes, and W. S. Caughey. 1991. Secondary structure-analysis of the scrapie-associated protein PrP 27–30 in water by infrared-spectroscopy. *Biochemistry.* 30:7672–7680.

Cheatham, T. E., J. L. Miller, T. Fox, T. A. Darden, and P. A. Kollman. 1995. Molecular-dynamics simulations on solvated biomolecular systems—the particle mesh Ewald method leads to stable trajectories of DNA, RNA, and proteins. *J. Am. Chem. Soc.* 117:4193–4194.

Cornell, W. D., P. Cieplak, C. L. Bayly, L. R. Gould, K. M. Merz, D. M. Ferguson, D. C. Spellmeyer, T. Fox, J. W. Caldwell, and P. A. Kollman. 1995. A 2nd generation force-field for the simulation of proteins, nucleic-acids, and organic-molecules. *J. Am. Chem. Soc.* 117:5179–5197.

DeMarco, M. L., and V. Daggett. 2004. From conversion to aggregation: protofibril formation of the prion protein. *Proc. Natl. Acad. Sci. USA.* 101:2293–2298.

Duan, Y., and P. A. Kollman. 1998. Pathways to a protein folding intermediate observed in a 1-microsecond simulation in aqueous solution. *Science.* 282:740–744.

Duan, Y., C. Wu, S. Chowdhury, M. C. Lee, G. Xiong, W. Zhang, R. Yang, P. Cieplak, R. Luo, T. Lee, J. Caldwell, J. Wang, and P. Kollman. 2003. A point-charge force field for molecular mechanics simulations of proteins based on condensed-phase quantum mechanical calculations. *J. Comput. Chem.* 24:1999–2012.

El Bastawissy, E., M. H. Knaggs, and L. H. Gilbert. 2001. Molecular dynamics simulations of wild-type and point mutation human prion protein at normal and elevated temperature. *J. Mol. Graph. Model.* 20:145–154.

Essmann, U., L. Perera, M. L. Berkowitz, T. Darden, H. Lee, and L. G. Pedersen. 1995. A smooth particle mesh Ewald method. *J. Chem. Phys.* 103:8577–8593.

Fox, T., and P. A. Kollman. 1998. Application of the RESP methodology in the parametrization of organic solvents. *J. Phys. Chem. B.* 102:8070–8079.

Fraunfelder, H., F. Parak, and R. D. Young. 1988. Conformational substates in proteins. *Annu. Rev. Biophys. Biophys. Chem.* 17:451–479.

Garcia, A. E., and K. Y. Sanbonmatsu. 2002. α-helical stabilization by side chain shielding of backbone hydrogen bonds. *Proc. Natl. Acad. Sci. USA.* 99:2782–2787.

Gsponer, J., P. Ferrara, and A. Caflisch. 2001. Flexibility of the murine prion protein and its Asp178Asn mutant investigated by molecular dynamics simulations. *J. Mol. Graph. Model.* 20:169–182.

Gu, W., T. Wang, J. Zhu, Y. Shi, and H. Liu. 2003. Molecular dynamics simulation of the unfolding of the human prion protein domain under low pH and high temperature conditions. *Biophys. Chem.* 104:79–94.

Guilbert, C., F. Ricard, and J. C. Smith. 2000. Dynamic simulation of the mouse prion protein. *Biopolymers.* 54:406–415.

Hornemann, S., and R. Glockshuber. 1998. A scrapie-like unfolding intermediate of the prion protein domain PrP(121–231) induced by acidic pH. *Proc. Natl. Acad. Sci. USA.* 95:6010–6014.

Huang, Z., S. B. Prusiner, and F. E. Cohen. 1996. Scrapie prions: a three-dimensional model of an infectious fragment. *Fold. Des.* 1:13–19.

James, T. L., H. Liu, N. B. Ulyanov, S. Farr-Jones, H. Zhang, D. Donne, K. Kaneko, D. Groth, L. Mehlhorn, and S. B. Prusiner. 1997. Solution structure of a 142-residue recombinant prion protein corresponding to the infectious fragment of the scrapie isoform. *Proc. Natl. Acad. Sci. USA.* 94:10086–10091.

Jorgensen, W. L., J. Chandrasekhar, J. D. Madura, R. W. Impey, and M. L. Klein. 1983. Comparison of simple potential functions for simulating liquid water. *J. Chem. Phys.* 79:926–935.

Kabsch, W., and C. Sander. 1983. Dictionary of protein secondary structure: pattern recognition of hydrogen-bonded and geometrical features. *Biopolymers.* 22:2577–2637.

Laio, A., and M. Parrinello. 2002. Escaping free-energy minima. *Proc. Natl. Acad. Sci. USA.* 99:12562–12566.

Liemann, S., and R. Glockshuber. 1999. Influence of amino acid substitutions related to inherited human prion diseases on the thermodynamic stability of the cellular prion protein. *Biochemistry.* 38:3258–3267.

Liu, H., S. Farr-Jones, N. B. Ulyanov, M. Llinas, S. Marqusee, D. Groth, F. E. Cohen, S. B. Prusiner, and T. L. James. 1999. Solution structure of Syrian hamster prion protein rPrP(90–231). *Biochemistry.* 38:5362–5377.

Lopez Garcia, F., R. Zahn, R. Riek, and K. Wüthrich. 2000. NMR structure of the bovine prion protein. *Proc. Natl. Acad. Sci. USA.* 97:8334–8339.

Marchi, M., and P. Procacci. 1998. Coordinates scaling and multiple time step algorithms for simulation of solvated proteins in the NPT ensemble. *J. Chem. Phys.* 109:5194–5202.

Monticelli, L., and G. Colombo. 2004. The influence of simulation conditions in molecular dynamics investigations of model β-sheet peptides. *Theor. Chem. Acc.* 112:145–157.

Mu, Y., D. S. Kosov, and G. Stock. 2003. Conformational dynamics of trialanine in water. 2. Comparison of AMBER, CHARMM, GROMOS, and OPLS force fields to NMR and infrared experiments. *J. Phys. Chem. B.* 107:5064–5073.

Nguyen, J. T., H. Inouye, M. A. Baldwin, R. J. Fletterick, F. E. Cohen, S. B. Prusiner, and D. A. Kirschner. 1995. X-ray-diffraction of scrapie prion rods and PrP peptides. *J. Mol. Biol.* 252:412–422.

Nosé, S. 1984. A molecular dynamics method for simulations in the canonical ensemble. *Molec. Phys.* 52:255–268.

Okur, A., B. Strockbine, V. Hornak, and C. Simmerling. 2003. Using PC clusters to evaluate the transferability of molecular mechanics force fields for proteins. *J. Comput. Chem.* 24:21–31.

Pan, K., M. Baldwin, J. Nguyen, M. Gasset, A. Serban, D. Groth, L. Mehlhorn, Z. Huang, R. J. Fletterick, F. E. Cohen, and S. B. Prusiner. 1993. Conversion of alpha-helices into beta-sheets features in the formation of the scrapie prion proteins. *Proc. Natl. Acad. Sci. USA.* 90: 10962–10966.

Parchment, O. G., and J. W. Essex. 2000. Molecular dynamics of mouse and Syrian hamster PrP: implications for activity. *Proteins.* 38:327–340.

Patra, M., M. Karttunen, M. T. Hyvönen, E. Falck, P. Lindqvist, and I. Vattulainen. 2003. Molecular dynamics simulations of lipid bilayers: major artifacts due to truncating electrostatic interactions. *Biophys. J.* 84:3636–3645.

Procacci, P., T. Darden, and M. Marchi. 1996. A very fast molecular dynamics method to simulate biomolecular systems with realistic electrostatic interactions. *J. Phys. Chem.* 100:10464–10468.

Procacci, P., T. A. Darden, E. Paci, and M. Marchi. 1997. ORAC: a molecular dynamics program to simulate complex molecular systems with realistic electrostatic interactions. *J. Comput. Chem.* 18:1848–1862.

Prusiner, S. B. 1982. Novel proteinaceous infectious particles cause scrapie. *Science.* 216:136–144.

Prusiner, S. B. 1996. Molecular biology and pathogenesis of prion diseases. *Trends Biochem. Sci.* 21:482–487.

Prusiner, S. B. 1998. Prions. *Proc. Natl. Acad. Sci. USA.* 95:13363–13383.

Prusiner, S. B., M. B. McKinley, K. A. Bowman, D. C. Bolton, P. E. Bendheim, D. F. Groth, and G. G. Glenner. 1983. Scrapie prions aggregate to form amyloid-like birefringent rods. *Cell.* 35:349–358.

Prusiner, S. B., M. P. McKinley, D. F. Groth, K. A. Bowman, N. L. Mock, S. P. Cochran, and F. R. Masiarz. 1981. Scrapie agent contains a hydrophobic protein. *Proc. Natl. Acad. Sci. USA.* 78:6675–6679.

Riek, R., S. Hornemann, G. Wider, M. Billeter, R. Glockshuber, and W. Wüthrich. 1996. NMR structure of the mouse prion protein domain PrP(121–231). *Nature.* 382:180–182.

Riek, R., G. Wider, M. Billeter, S. Hornemann, R. Glockshuber, and K. Wüthrich. 1998. Prion protein NMR structure and familial human spongiform encephalopathies. *Proc. Natl. Acad. Sci. USA.* 95:11667–11672.

Saito, M. 1994. Molecular-dynamics simulations of proteins in solution—artifacts caused by the cutoff approximation. *J. Chem. Phys.* 101: 4055–4061.

Sekijima, M., C. Motono, S. Yamasaki, K. Kaneko, and Y. Akiyama. 2003. Molecular dynamics simulation of dimeric and monomeric forms of human prion protein: insight into dynamics and properties. *Biophys. J.* 85:1176–1185.

Stahl, N., and S. B. Prusiner. 1991. Prions and prion proteins. *FASEB J.* 5:2799–2807.

Swietnicki, W., M. Morillas, S. G. Chen, P. Gambetti, and W. K. Surewicz. 2000. Aggregation and fibrillization of the recombinant human prion protein huPrP90–231. *Biochemistry.* 39:424–431.

Swietnicki, W., R. Petersen, P. Gambetti, and W. K. Surewicz. 1997. pH-dependent stability and conformation of the recombinant human prion protein PrP(90–231). *J. Biol. Chem.* 272:27517–27520.

Tuckerman, M., B. J. Berne, and G. J. Martyna. 1992. Reversibile multiple time scale molecular-dynamics. *J. Chem. Phys.* 97:1990–2001.

Turk, E., D. B. Teplow, L. E. Hood, and S. B. Prusiner. 1988. Purification and properties of the cellular and scrapie Hamster prion proteins. *Eur. J. Biochem.* 176:21–30.

Wille, H., M. D. Michelitsch, V. Génebaut, S. Supattapone, A. Serban, F. E. Cohen, D. A. Agard, and S. B. Prusiner. 2002. Structural studies of the scrapie prion protein by electron crystallography. *Proc. Natl. Acad. Sci. USA.* 99:3563–3568.

Wolf, D., P. Keblinski, S. R. Phillpot, and J. Eggebrecht. 1999. Exact method for the simulation of Coulombic systems by spherically truncated, pairwise r^{-1} summation. *J. Chem. Phys.* 110:8254–8282.

Zahn, R., A. Liu, T. Lührs, R. Riek, C. von Schroetter, F. Lopez Garcia, M. Billeter, L. Calzolai, G. Wider, and K. Wüthrich. 2000. NMR solution structure of the human prion protein. *Proc. Natl. Acad. Sci. USA.* 97: 145–150.

Zaman, M. H., M.-Y. Shen, R. S. Berry, K. F. Freed, and T. R. Sosnick. 2003. Investigations into sequence and conformational dependence of backbone entropy, inter-basin dynamics and the Flory isolated-pair hypothesis for peptides. *J. Mol. Biol.* 331:693–711.

Ziegler, J., H. Sticht, U. C. Marx, W. Müller, P. Rösch, and S. Schwarzinger. 2003. CD and NMR studies of prion protein (PrP) helix 1: novel implications for its role in the $PrP^{C} \rightarrow PrP^{SC}$ conversion process. *J. Biol. Chem.* 278:50175–50181.

Zou, W. Q., and N. R. Cashman. 2002. Acidic pH and detergents enhance in vitro conversion of human brain PrP^{C} to a PrP^{SC}-like form. *J. Biol. Chem.* 277:43942–43947.